**Naval Research Laboratory**

**Washington, DC 20375-5320**

**NRL/FR/7210--07-10,149**

# Radiometric Characterization of a New Photovoltaic Cell Unit for Powering Modulating Retroreflectors

XIAOLEI ZHANG
JAMES MURPHY

*Radio, IR, and Optical Sensors Branch*
*Remote Sensing Division*

G. CHARMAINE GILBREATH

*Free Space Photonics Communications Office*
*Information Technology Division*

June 19, 2007

# REPORT DOCUMENTATION PAGE

*Form Approved*
*OMB No. 0704-0188*



| **1. REPORT DATE** *(DD-MM-YYYY)* | **2. REPORT TYPE** | **3. DATES COVERED** *(From - To)* |
|---|---|---|
| 19-06-2007 | Formal Report | 12/05 - 09/06 |

**4. TITLE AND SUBTITLE**

Radiometric Characterization of a New Photovoltaic Cell Unit for Powering Modulating Retroreflectors

**5a. CONTRACT NUMBER**

**5b. GRANT NUMBER**

**5c. PROGRAM ELEMENT NUMBER**

**6. AUTHOR(S)**

Xiaolei Zhang, James L. Murphy, and G. Charmaine Gilbreath

**5d. PROJECT NUMBER**
72-6388

**5e. TASK NUMBER**
JON 6388-07

**5f. WORK UNIT NUMBER**

**7. PERFORMING ORGANIZATION NAME(S) AND ADDRESS(ES)**

Naval Research Laboratory, Code 7210
4555 Overlook Avenue, SW
Washington, DC 20375-5320

**8. PERFORMING ORGANIZATION REPORT NUMBER**

NRL/FR/7210--07-10,149

**9. SPONSORING / MONITORING AGENCY NAME(S) AND ADDRESS(ES)**

Office of Naval Research
Suite 1425
875 North Randolph Street
Arlington, VA 22203-1995

**10. SPONSOR / MONITOR'S ACRONYM(S)**
ONR

**11. SPONSOR / MONITOR'S REPORT NUMBER(S)**

**12. DISTRIBUTION / AVAILABILITY STATEMENT**

Approved for public release; distribution is unlimited.

**13. SUPPLEMENTARY NOTES**

**14. ABSTRACT**

We describe the experimental procedures and results of a detailed radiometric characterization of a new photovoltaic (PV) wafer unit intended for powering the Multiple Quantum Well (MQW) Modulating Retroreflector (MRR) using natural sunlight and/or system laser light as energy input, to enable autonomous operation of free-space optical data link using the MQW MRR. Our initial measurements show that the PV wafer unit has an average power conversion efficiency of 7% to 8% over the entire visible-to-IR wavelength range from 200 nm to 3500 nm, and a conversion efficiency around 40% at the 1550 nm laser frequency. Comparisons of the different methods for radiometric characterization of the PV wafer unit are also given.

**15. SUBJECT TERMS**

Optical interferometry  Infrared interferometry
Satellite imaging

| **16. SECURITY CLASSIFICATION OF:** | | | **17. LIMITATION OF ABSTRACT** | **18. NUMBER OF PAGES** | **19a. NAME OF RESPONSIBLE PERSON** |
|---|---|---|---|---|---|
| | | | | | Xiaolei Zhang |
| **a. REPORT** | **b. ABSTRACT** | **c. THIS PAGE** | UL | 16 | **19b. TELEPHONE NUMBER** *(include area code)* |
| Unclassified | Unclassified | Unclassified | | | (202) 404-2389 |

**Standard Form 298 (Rev. 8-98)**
**Prescribed by ANSI Std. Z39.18**

## CONTENTS

# RADIOMETRIC CHARACTERIZATION OF A NEW PHOTOVOLTAIC CELL UNIT FOR POWERING MODULATING RETROREFLECTORS

## 1. INTRODUCTION

The Multiple Quantum Well (MQW) Modulating Retroreflector (MRR) technology [1,2] was developed to enable a free-space optical communication node. The motive for integrating a monolithically integrated photovoltaic (PV) module [3] as a power source into the MRR is that the whole unit could become a stand-alone, miniature free-space communication node. The PV module consists of many individual solar cells monolithically integrated on a single substrate, thus allowing the efficient conversion of both the natural sunlight and system laser light into the range of voltages and currents needed to operate the MRR. Initial benchtop demonstration of the operational system of the PV module is described in Ref. 3. This report presents a detailed radiometric characterization of the whitelight and laser light conversion efficiencies of the PV wafer unit.

The report is organized as follows: Section 2 describes the different options for doing the required radiometry tests, based on available technologies and instruments, and gives the rationales for the final adopted methodologies employed in this work. Section 3 describes the first set of whitelight power-conversion-efficiency measurements using a standard calibrated spherical radiance source from Oriel. Section 4 describes the measurement of the whitelight conversion efficiency using a charge-coupled device (CCD) camera with a calibrated sensitivity (with the calibration procedure and results described in the Appendix), and compares it with the efficiency measured using the method given in Section 3. Section 5 describes the measurement of the PV wafer conversion efficiency at the 1550 nm laser frequency. Finally, Section 6 summarizes the conclusion of this work.

## 2. OPTIONS FOR RADIOMETRIC CHARACTERIZATION

Since during the intended usage the PV wafer unit would be powered either by natural sunlight, or system laser light at 1550 nm, or a combination of both, we have designed the tests to explore the power conversion efficiencies in these different operating modes.

### 2.1 Choices of Source and Configuration for the Whitelight Test

The whitelight flux level we are interested in for the purpose of characterizing the PV wafer power conversion efficiency ranges from 1 solar irradiance (=136.61 mW/cm2) to a fraction of the solar irradiance.

One of the available sources is a Labsphere Unisource 4000 integrating sphere enclosing 10 different quartz halogen lamps. The lamps are operated at a blackbody temperature of about 3000 K. The sphere is 91 cm (36 in.) in diameter, and has an exit port of 35.5 cm (14 in.) in diameter. The output of this source has a Lambertian distribution (uniform radiance with respect to angles). This source has been previously calibrated by another group at the NRL with 10 nm bandwidth using an Optronics single grating

Manuscript approved October 10, 2006.

spectrometer [4]. The calibrated radiance covers the spectral range from 200 to 3500 nm. The dual characteristics, uniform illumination in angles and the availability of precision-calibrated radiance from one to ten lamp settings, provide an ideal choice for us in terms providing a known standard of energy input into the PV wafer.

As for the test configuration, two possible choices have been considered. First of all, the PV wafer can be directly placed in the illuminated area of the exit aperture of the integrating sphere. Measured I-V response from the PV wafer can be compared with the estimated energy input based on the radiance of the source at the lamp setting used, the distance from the exit aperture, and the active area of the PV wafer. Secondly, we could use a lens to "focus" the emergent light from the sphere source, and place the PV wafer unit at the focal area of the lens. The configuration has the advantage that the flux level is independent of the distance of the lens from the exit port of the source, as long as the PV wafer is placed within the illuminated aperture of the source. The disadvantage of this second configuration is that the available flux with each lamp setting is cut down significantly, due to the much smaller area of the lens (in our case, the lens is approximately 80 mm in diameter) compared to the area of the exit port of the source. In addition the lens inserts some reflection and absorption losses as well.

In addition to estimating the input flux to the PV wafer based on the known source radiance, we also used a CCD camera with known calibrated response to estimate the input flux. These two approaches are compared and will be described later in the text.

### 2.2 Choices of Source and Test Configuration for the 1550 nm Laser Test

The source assembly for the laser radiometry characterization was made in-house, and has a maximum output power of 2.2W, and is fiber-coupled (see Section 5 for more detailed description of the laser source and test assembly). The output light is allowed to naturally expand and to illuminate the PV wafer at a distance large enough so the flux density on the 2-in. PCV chip is approximately homogeneous.

In order to measure the 1550-nm laser flux at the location of the PV wafer, we will need a different detector than the whitelight CCD camera. The options of both the IR array cameras and single-pixel PIN diodes have been explored. The PIN diode in principle could be the least expensive solution, and its linearity under a properly selected bias is also known to be good. However, the commercial off-the-shelf version of the PIN diode only provides a generic calibration curve for a given batch, and not for each individual diode in the batch. Furthermore, the calibration curves are invariably obtained under the condition of under-filling the active area of the InGaAs chip. We have contacted NIST Gaithersburg diode calibration branch, and were told that to do individual diode calibration under the under-filling condition usually costs about $3400 per diode, to obtain the entire spectral response curve (and no discount for a single wavelength). To perform an overfilling, radiance-response measurement (as would be needed for our type of measurement where the beam to be measured is much larger than the diode), the cost is between $7000 and $10,000 per diode. Tom Larason from NIST also informed us that customers had reported that in the overfilling condition, single-pixel diodes had exhibited nonlinear responses to power during actual usage, likely due to the inhomogeneities at the edges of the active area, The bottom line is that the single diode is generally not meant for beam-sampling type of measurement. Rather it is meant to be used under the condition that the input beam is only partially filling the active area (the typical case that the NIST team usually encounters is that a test beam would have 1 mm diameter, with less than 5 degree of angular spread, and the diode to be tested is expected to have an active area of at least 5 mm in diameter).

A second possible choice for the detector for 1550 nm laser is a calibrated (or calibratable) IR array camera. The InGaAs ones have the most dynamic range and power-handling capability, but they tend to

be the most costly as well. The two major vendors (FLIR/Indigo system with their Phoenix and Alpha models, and Sensors Unlimited with their SY series), sell InGaAs array cameras with prices ranging between $22,000 and $40,000 per camera, depending on the format of the array, the wavelength coverage, and whether or not it has the CameraLink interface. Another vendor, Spiricon, sells a phosphor-enhanced CCD camera that works at 1550 nm (model SP-1550M). The cost is significantly less (camera, frame grabber, and software together cost around $5000). It has a format of 640 × 480 and can do 30 frames/second. The software that comes with the camera also provides corrections to the nonlinearity in the phosphor fluorescent conversion.

In the end, we selected a calibrated laser power meter with a head active area of 5 mm on a side (25 $mm^2$ total area). This power head is known to have linear responses under the overfilling conditions that we use.

## 3. WHITELIGHT RADIOMETRIC CHARACTERIZATION OF THE PV WAFER USING THE INTEGRATING-SPHERE RADIANCE SOURCE

Figure 1 shows the radiance curve for the existing whitelight source enclosed in an integrating sphere. The values were measured/calibrated by another group at NRL between 300 nm and 2500 nm to an accuracy on the order of 2%. Extrapolation of the curve has been done to fill the range between 200 nm to 300 nm, and between 2500 nm and 3500 nm. In Fig. 2 we present the solar spectrum in the corresponding spectral range, both within and above the Earth atmosphere (and for the former including the absorption bands caused by various atmosphere molecules). It can be seen that the spectral radiance curve of the sphere resembles that of the Sun (even though it is not specified exactly as a solar spectral source), so the measurement we made using this source of the whitelight power conversion efficiency of the PV wafer should be close to the efficiency of conversion of solar power.

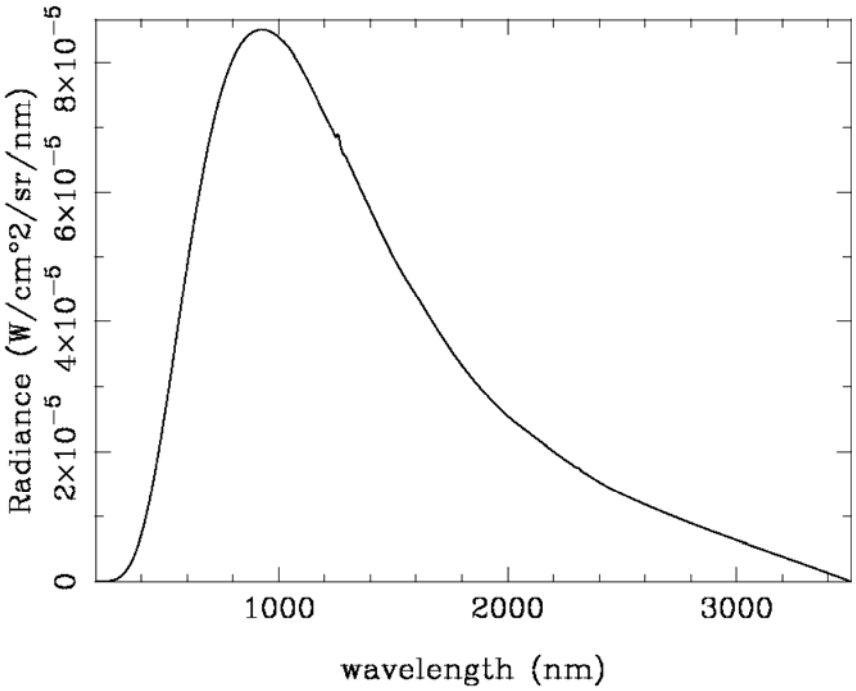


Fig. 1 — Radiance of the Oriel Integrating Sphere Radiance Source, with 10 lamps turned on

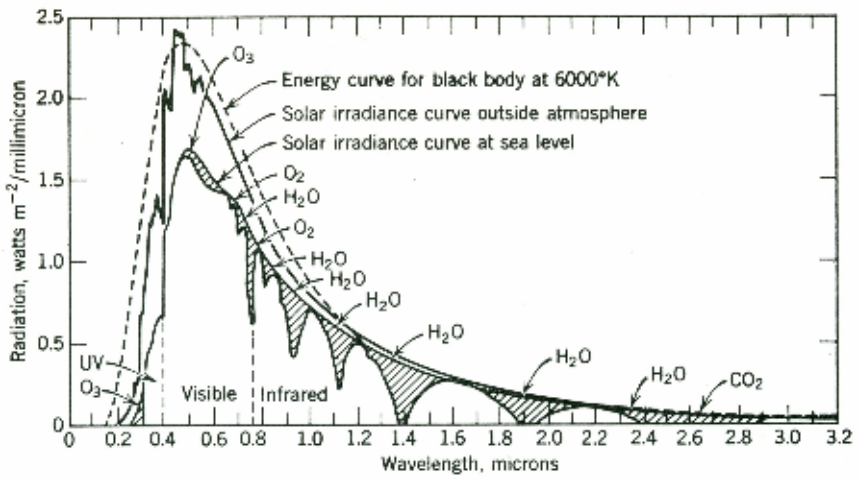


Fig. 2 — Spectrum of the Sun in the visible and IR range (from *Handbook of Geophysics* [5])

Using this known radiance curve, for our test configuration (see Fig. 3), which is set up at a height of 10.5 above the optical table, the received power by the PV wafer unit can be calculated from

$$Power = \int_{200}^{3500} (Radiance) \bullet (Area) \bullet (Solid\,Angle) d\lambda \tag{1}$$

where Radiance is the calibrated radiance of the source at each wavelength, Area is the effective active area of the PV wafer, and Solid Angle is the solid angle subtended by the source sphere viewed from the location of the PV wafer.

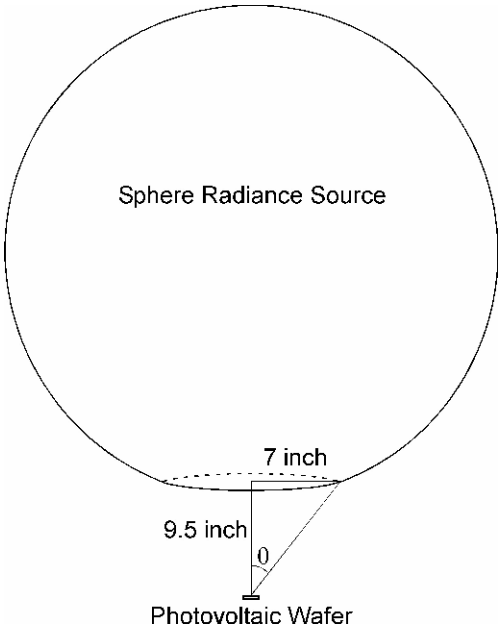


Fig. 3 — Schematic of the test configuration using a sphere radiance source

For our test setup, the PV wafer has an active area of 0.0011 m$^2$, and is situated from the source aperture at a distance of 9.5 in., which results in a solid angle of the source of

$$\Omega = 2\pi\left(1-\cos\theta\right) = 1.225,$$

where $\theta$ is obtained from $\theta = \tan^{-1}(7/9.5)$. In performing the above integral, we can see that the received power by the PV wafer over the entire visible-infrared waveband of the source is 1410 mW, or a power density of 127.26 mW/cm$^2$, which is just under 1 solar irradiance, as we would have desired. We chose the current test configuration as the primary one because the re-imaging configuration with a lens was found to result in about a factor of 10 loss in flux at the location of the PV wafer if it is located as the lens focus.

In order to derive the PV wafer power conversion efficiency, apart from the above input power measurement/calculation, we need also to measure the output power from the PV wafer under the same illumination conditions. For this purpose, we used a Keithley Model 2425 SourceMeter to measure the I-V curve. The measurements were made by varying the load voltage across the photovoltaic device and measuring the resulting current.

Figure 4 shows such measured curves under 1 to 10 lamps source illumination, and various bias conditions.

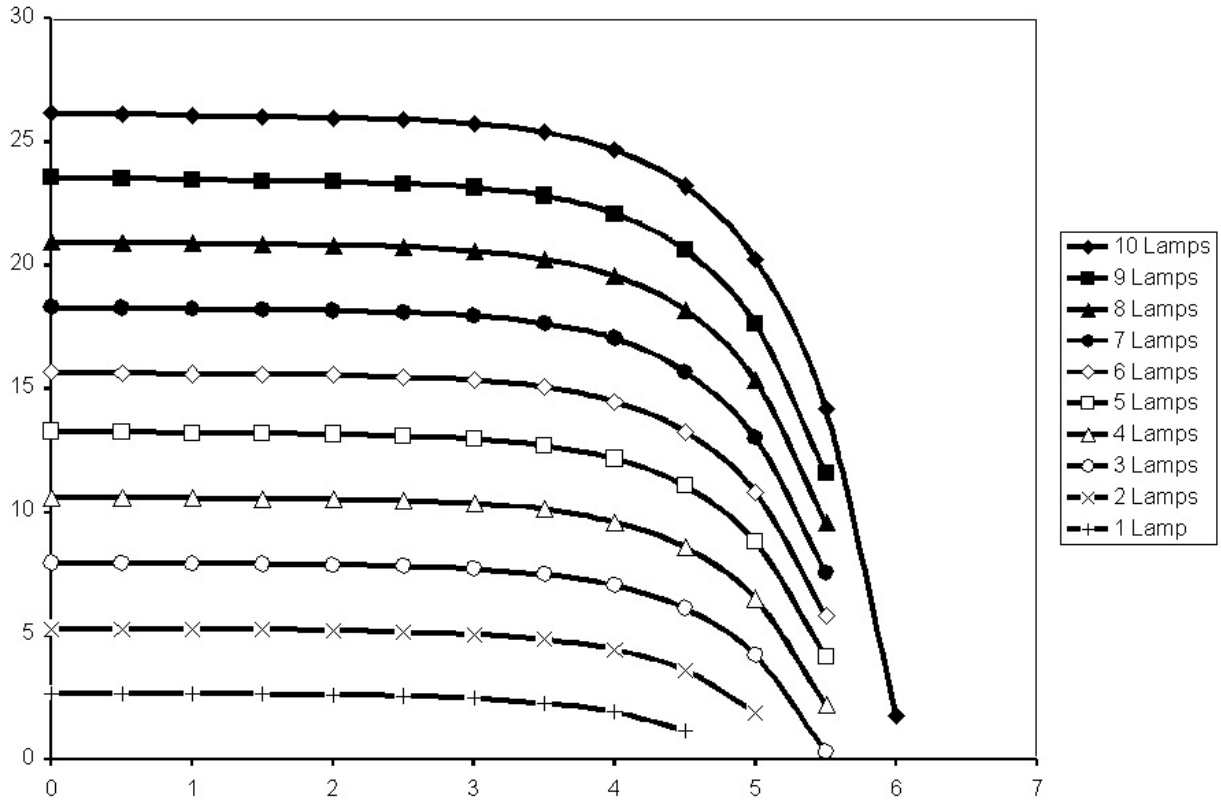


Fig. 4 — Measured I-V curves of the photovoltaic wafer under 1 to 10 lamps source illumination

From this figure, we can calculate the power output at each setting by multiplying the I and V values corresponding to each data point. For every lamp setting, we find that there is a maximum power output point from these I-V products. For the case of 10 lamps of illumination, the maximum power output in

our test configuration is 103.5 mW. Using the calculated input power of 1410 mW, we arrived at the power conversion efficiency of 7.3% for a light source that has a similar spectral power distribution in the visible and IR band as shown in Fig. 1.

## 4. WHITELIGHT RADIOMETRIC CHARACTERIZATION OF THE PV WAFER USING A CCD CAMERA

The power conversion efficiency measurement and calculation in the last section were done under the assumption that the radiance curve of the source over the spectral range of interests was accurately known or calibrated. Even though we trust the previous measurements of the other group that conducted the radiance calibration, we have decided to verify the results through our own irradiance or flux measurement at the location where the PV wafer is posited.

Ideally, such a radiometry measurement should be done with a detector or camera that has both the visible and infrared response. Due to cost considerations as described in Section 2, we have decided to use an existing visible light CCD camera, of model Adimec 1000-M, to perform this radiometry calibration of the source. The quantum efficiency (QE) of the CCD is given in Fig. 5. Note that the manufacturer only supplied the QE in the range of 300 to 1000 nm. Beyond that range, the values in the figure are extrapolated from knowledge of typical CCD chip performance.

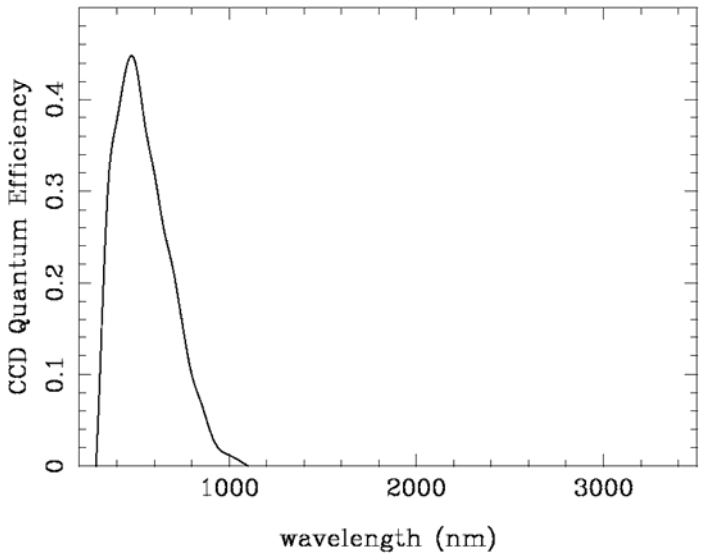


Fig. 5 — Quantum efficiency of the Adimec 1000-M CCD camera

From Fig. 5, it is obvious that this CCD camera does not have significant responses beyond the visible region. However, if we could reasonably assume that the shape of the radiance curve of the source is known, and only the absolute value of its calibration needs to be determined, we can use the CCD-measured flux to infer the total flux in the visible-IR region as radiated by the source.

### 4.1 Vignetting Correction

Before presenting the measurement and calculation of the CCD radiometry, we first point out that there is an additional complicating factor we need to consider when using the existing CCD camera to

measure the flux density at the nominal location of the PV wafer, using the sphere radiance source. This is the vignetting of the light rays from the sphere source aperture, which would reach the PV wafer unimpeded if the wafer were located at the entrance aperture of the CCD camera. However, since the CCD chip is mounted receded within the aperture, these rays are partially blocked by the entrance aperture of the CCD.

In order to determine the effect of this vignetting (which results in a reduction of the effective solid angle that can be perceived by the CCD), we used the configuration shown in Fig. 6(a). We measured the flux level using the CCD (with 10 lamps on in the source), as well as the power output of the PV wafer, first without the baffle and the lens; and then repeated these two measurements with the baffle and the lens (with the CCD and the PV wafer this time placed at the focal region of the lens). The CCD count rates in these two sets of measurements differ by a factor of about 120, and the power output from the PV wafer differ by a factor of 240. The additional factor of 2 is from the vignetting of the rays of the sphere source by the CCD aperture tube due to the recessing of the CCD chip from its aperture as shown in Fig. 6(b). This reduces the effective solid angle of the source as viewed by the CCD by a factor of 2, compared to the solid angle as viewed by the PV wafer.

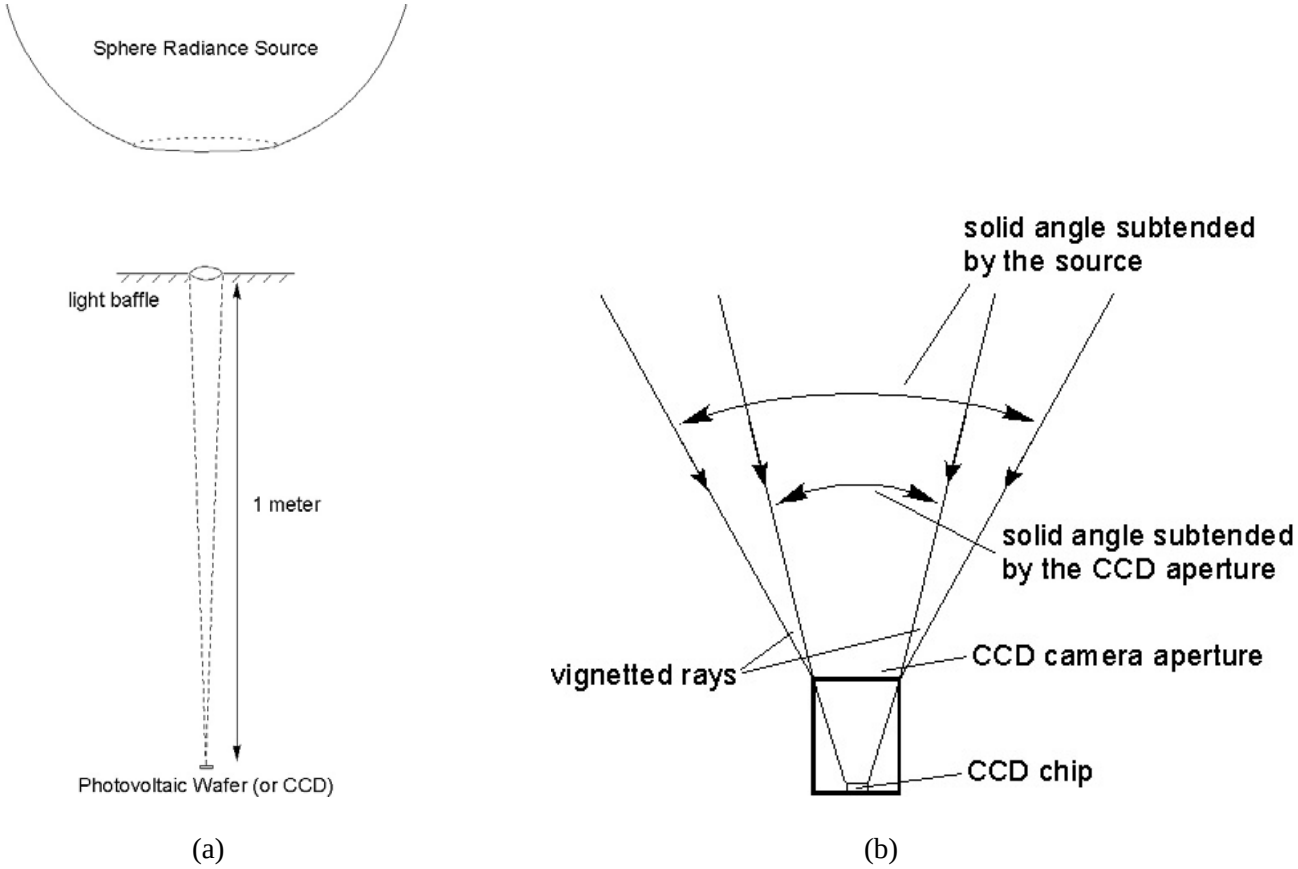


(a) (b)

Fig. 6 — (a) Test configuration for determining the CCD vignetting factor; (b) schematic diagram of vignetting by the CCD camera aperture

### 4.2 Using the Digital Gain Information and the QE of the CCD

One piece of information we were able to obtain from the vendor through email, which was not contained in the original camera specification manual, was that the digital gain of the CCD chip was about 38000 electrons for full-scale. Since we are running the camera in the 8-bit mode, then 255 = full scale = 38000 electrons, or 1 count = 148 electrons.

From this information, we can calculate the expected integrated count rates at the CCD as

$$count\ rate = \int_{200}^{3500} \frac{I(\lambda)\cdot\Omega\cdot Area_{ccd}\cdot QE(\lambda)}{h\nu\cdot 148\cdot f_{vignette}}\, d\lambda \tag{3}$$

where $I(\lambda)$ is the nominal radiance curve of the source we had used in the last section; $\Omega$ is the solid angle subtended by the source exit aperture to the CCD (which is placed at the same location as the PV wafer, as shown in Fig. 2), and $\Omega = 1.225$; $Area_{ccd}$ is the area of the CCD chip, which is the sum of 1000 by 1000 pixels each of 7.4 μm × 7.4 μm, or $5.48\times10^{-5}$ m$^2$; and $f_{vignette}\approx 2$ is a vignetting factor to account for the location of the CCD chip about an inch back from the aperture of the camera (therefore, not all of the rays from the solid angle subtended by the source can be detected by the CCD, whereas all these rays can reach the 2-in. diameter PV wafer during its I-V curve measurement). The vignetting factor reduced the effective solid angle of the source as perceived by the CCD by a factor of 2.

Carrying out the above integration, we obtain that the expected count-rate is about $3.6 \times 10^{13}$ per second, whereas the actual read-out from the CCD was about $3.5 \times 10^{13}$ per second. These numbers are in very good agreement, and we thus conclude that the sphere radiance source calibration we had used before is accurate as confirmed by the current CCD measurements (as well as by those of Section 4.3).

### 4.3 Using the CCD QE Curve and the Average Photopic Response Curve

This part of the radiometry calibration was initially carried out prior to the calibration verification described in Section 4.2, since in the CCD camera manual the sensitivity was specified as "approximately 5.5 lux for 100% video, 33 ms integration time, 3200 K light source with BG-38-1-mm color glass filter," in addition to the quantum efficiency curve quoted above. This averaged sensitivity was cumbersome to use, since, as shown in Fig. 7, the transmission curve of the BG-38 filter has a finite width. Furthermore, the human eye response curve, shown in Fig. 8, which was used in the lux unit definition, makes the unambiguous conversion between the above-average sensitivity measured in photometric units and the spectral sensitivity we seek nearly impossible, because of the non-uniqueness of the regression, in general, from the photometric quantities to their corresponding radiometric quantities. We have struggled with this and eventually obtained an approximate mutual consistency of sensitivity measurements through length unit conversions and rescaling.

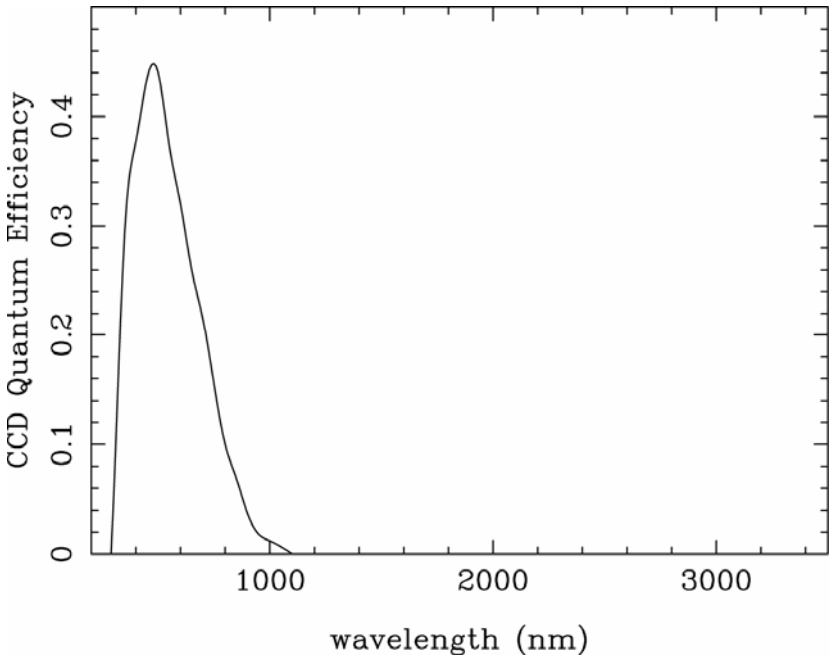


Fig. 7 — Transmission curve of the BG-38 filter used during the calibration of the Adimec 1000-M CCD camera

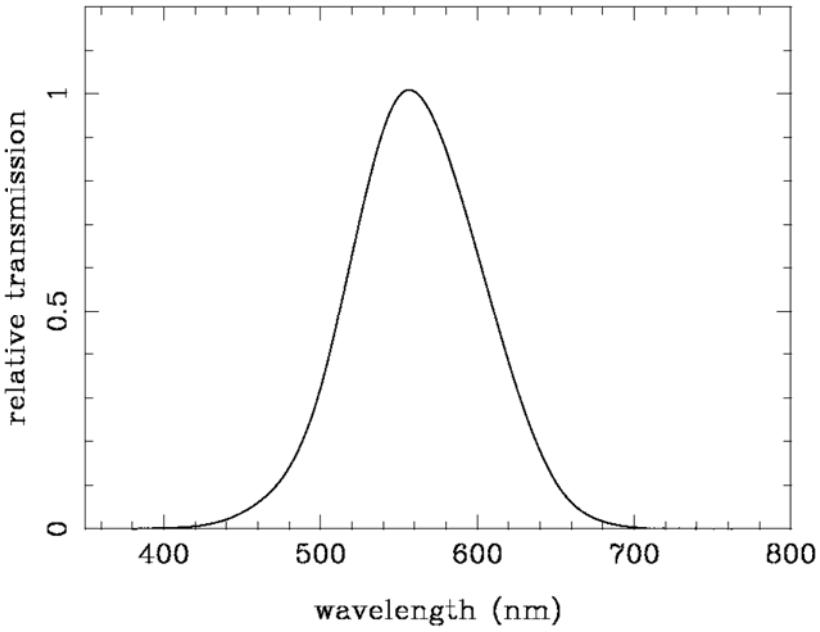


Fig. 8 — Human eye response curve as used in the definition of lumen and lux units

However, after obtaining the digital gain from the vendor at the very end of our experiment, such mutual conversion of sensitivity measured in different units becomes more straightforward (since it becomes a forward problem instead of a regression problem). Now, all we need to do is to confirm that with a T = 3200 K blackbody source, which has the spectral energy distribution given by

$$U(\lambda,T)=\frac{8\pi hc\lambda^{-5}}{e^{hc/\lambda kT}-1} \tag{4}$$

as shown in Fig. 9, that the sensitivity we calculate using $U(\lambda,T)$, the filter transmission curve $BG38(\lambda)$, the human eye response curve $y(\lambda)$, and the CCD quantum efficiency curve $QE(\lambda)$, gives the same result as quoted by the manufacturer's above number.

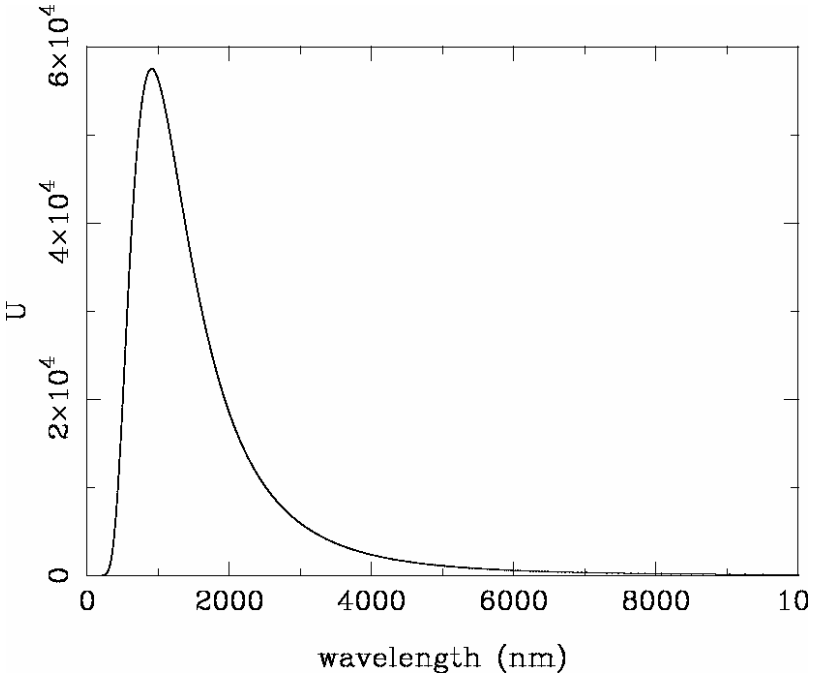


Fig. 9 — 3200 K blackbody radiation curve

The Adimec 1000M can be used in both the 10-bit and 8-bit modes. Since we have used the camera in the 8-bit mode for all of our usage of it so far, the expected sensitivity for the 8-bit mode is

$$Sensitivity\left(\lambda_{cal}\right)_{8-bit}=\frac{256}{5.5}\times 33=1536\ counts/lux/s \tag{5}$$

To calculate an average sensitivity in the corresponding wavelength range of the filter using the above curves and digital gain, so as to compare with the quoted sensitivity above, we note first some conversion factors between photometric and radiometric units. In the photometric unit convention, 1 lux = 1 lumen/$m^{-2}$. Also, the definition of lumen is such that 1 W of optical flux at 555 nm gives the same physical sensation as do 680 lumen. Defining $K_m$ = 680 lm/W, we have that at other wavelengths

$$K_\lambda = K_{mY\lambda} = 680_{Y\lambda}\left[lm/W\right], \tag{6}$$

where the normalized conversion factor y(λ) is a bell-shaped curve with wavelengths (see Fig. 8) peaked at 555 nm with value 1, and which drops to zero at the two ends around 400 and 700 nm, respectively.

With this information we can now calculate the conversion factor between the effective incident flux rate and the integrated count rate measured by the CCD (which has a linear pixel size of 7.4 μm). The flux in the unit of lux is calculated from

$$f_{lux}(lux) = \int_{200}^{1100} U(\lambda, T) \cdot BG38(\lambda) \cdot y(\lambda) \cdot 680 d\lambda \,, \tag{7}$$

and the counts per second measured by the CCD under the same flux condition is calculated from

$$counts/s = \int_{200}^{1100} \frac{U(\lambda, T) \cdot QE(\lambda) \cdot BG38(\lambda)}{148 \cdot (hc/\lambda)} \cdot Area_{ccd} d\lambda \,. \tag{8}$$

From the above two calculations, we obtain that the calculated sensitivity conversion factor is 1296 counts/lux/s. This number is about 18% higher than the manufacturer-quoted average sensitivity number. But considering the uncertainty in the factory test setup and the variations in the filter response, lux meter, source intrinsic properties, etc., we consider the agreement satisfactory.

Because the digital gain calculation of Section 4.2 gives a better agreement with our calibration using the sphere radiance source (which is believed to be itself calibrated to between 2% and 5% accuracy), we consider the discrepancy to be mainly contributed by the error in the average sensitivity as quoted by the vendor, and not in the digital gain.

## 5. CHARACTERIZATION OF THE PV WAFER POWER CONVERSION EFFICIENCY AT 1550 NM SYSTEM LASER FREQUENCY

We have conducted the 1550 nm laser power conversion efficiency measurement for the PV wafer using a laser source unit built in-house using mostly commercial parts, a Newport laser power meter (for measuring input power), and the same SourceMeter used in the previous whitelight test to measure the I-V curve, and, thus the output power, from the PV wafer.

The seed laser used was a JDS Uniphase Model CQF935/508 1550-nm laser diode with a maximum output power of 50 mW. The seed laser was coupled into a Lucent Erbium/Yttrium Doped Fiber Amplifier (EDFA) (there is no model number associated with this; it was built here at NRL) with a maximum output power of 2.2 W at 12.8 A drive current. The actual output power used was 600 mW measured at the output of the fiber.

The optical power meter used was a Newport Multi Function Optical Power Meter Model 2835-C. We used two sensor heads for the experiment: a Model 818-IS-1 Universal Fiber Optic Detector was used to measure the total output power of the laser source, and a Model 818-IR Infrared Detector was used to measure the laser power at the photovoltaic wafer. Both units have an NIST traceable calibration that is integrated into the sensor.

For this test we made sure that the location of the PV wafer was far enough away (in this case 39 in.) from the fiber output of the laser source assembly so that the illumination on the 2-in. PV wafer was roughly homogeneous. This was confirmed by power density measurement using a small Newport IR detector diode at the different locations on the 2-in. area where the wafer was located. We obtained a reading of 1.17 mW at 0.5 in. to the right of the nominal center of the wafer, and 0.975 mW at 0.5 inch to the left of the nominal center of the wafer. Since the detector diode was about 5 mm on a side, this gave an averaged power density of 4.29 mW/cm$^2$ over the entire 2-in. wafer.

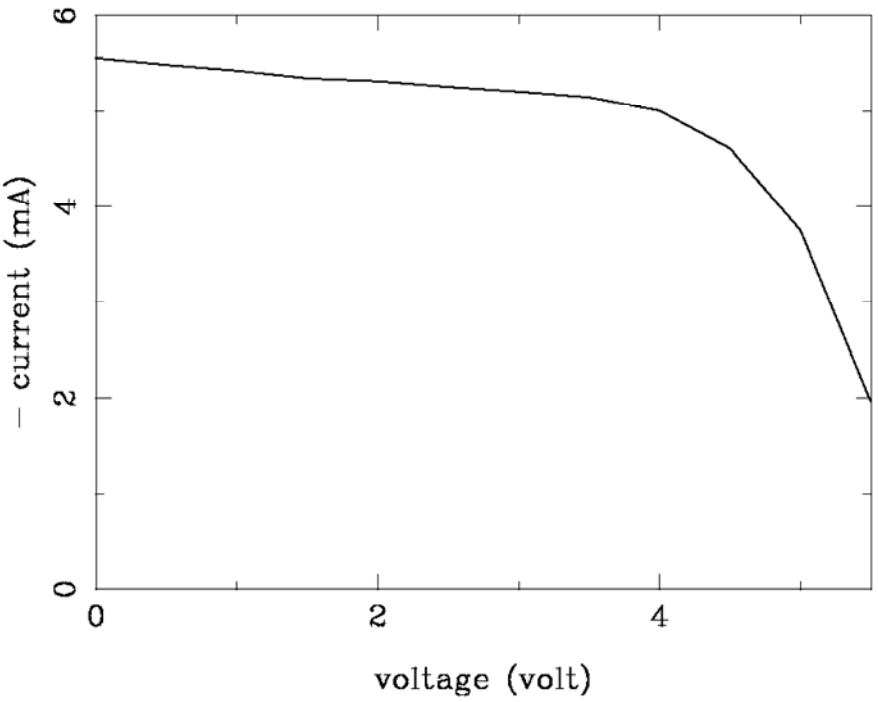


Fig. 10 — Voltage-current curve measured for the PV wafer under illumination by a 1550-nm laser source situated 39 in. away

The maximum output power from the PV wafer, calculated from the above curve, is 20.75 mW. The input power is obtained by measuring the power flux density at the PV wafer, which is determined to be 4.29 mW/cm$^2$, or 47.53 mW of total input power on the 11.08 cm$^2$ of the PV wafer active area.

The power conversion efficiency at the 1550 nm laser frequency was thus 43%. This is much higher than the average whitelight power conversion efficiency, but such a difference between the 1550 nm and average whitelight and efficiency had been obtained before by others in the community.

## 6. SUMMARY

We conducted a thorough radiometric characterization of the power conversion efficiency of a new photovoltaic wafer unit intended for providing the operational power, through the conversion of sunlight and system laser light into electrical currents and voltages, for the autonomous operation of the Multiple Quantum Well Modulating Retroreflector. The results of the test show that when used alone, the PV wafer has an average sunlight conversion efficiency in the 200 to 3500 nm range of around 7% to 8%, and a laser light conversion efficiency at 1550 nm of around 43%. When the laser and whitelight are used together to power the PV wafer, we expect a first-order linear dependence of total conversion efficiencies.

## REFERENCES

1. G.C. Gilbreath, S.R. Bowman, W.S. Rabinovich, C.H. Merk, and H.E. Senasack, “Modulating Retroreflector Using Multiple Quantum Well Technology,” U.S. Patent No. 6, 154,299, awarded November, 2000.

2. G.C. Gilbreath, T.J. Meehan, R. Walters, S. Mozersky, M. Ferraro, S.R. Messenger, and W.S. Rabinovich, "Multiple Quantum Well Retromodulators for Low Power, Covert Infrared Data Links," Proceedings of Association for Unmanned Vehicles Society International, Baltimore, MD, August 1-2, 2001.

3. R.J. Walters, J.L. Murphy, W.S. Rabinovich, G.C. Gilbreath, D.M. Wilt, M.A. Smith, M.J. Krasowski, P.P. Jenkins, D. Scheiman, J.H. Warner, S.R. Messenger, J.R. Lorentzen, and G.P. Summers, "Photovoltaically Powered Modulating Retroreflectors," Proceedings of the SPIE Vol. 5550, Free-Space Laser Communications IV, J.C. Ricklin and D.G. Voelz, eds., Bellingham, WA, 2004.

4. D.R. Korwan, J.H. Bowles, W.A. Snyder, M.R. Corson, and C.O. Davis, "Radiometric Calibration of a Coastal Ocean Hyperspectral Imager Using a Blue Enhanced Integrating Sphere," poster, 9th International Conference on New Developments and Applications in Optical Radiometry, Davos, Switzerland, October 2005.

5. U.S. Air Force, *Handbook of Geophysics* (The Macmillan Co., New York, 1960).